Journal of Porous Materials
https://doi.org/10.1007/s10934-021-01118-9

Monoliths of Tio2-SiO2: synthesis, characterization and photocatalytic activity

Manuel Robles-Melgarejo[1] · Jaime Espino-Valencia[1] · Reyna Natividad-Rangel[2] · Santiago José Guevara-Martínez[3] · José Luis Rico-Cerda[1] · Ricardo Rangel-Segura[1]

Accepted: 25 June 2021

Abstract
Monoliths of TiO_2-SiO_2 were synthesized by the Evaporation-Induced Self-Assembly (EISA) method and tested in the photocatalytic degradation of 4-chlorophenol. The way of adding the titanium precursor and the calcination conditions (temperature and air flow) were studied and were found to be key parameters in determining the physical, morphological, structural and photocatalytic properties. Opaque monoliths with crystalline anatase and rutile structures were obtained after calcination when the titanium precursor was directly added during the Si sol synhesis. Under another approach, adding the titanium precursor as a Ti sol to the Si sol, transparent materials with amorphous or small crystal size structures were produced. All monoliths presented mesoporous structures with specific surface areas in the value range of 528–813 m^2g^{-1}. The highest values corresponded to those materials calcined under air flow. The materials were tested in the 4-chlorophenol photocatalytic activity. After testing, a significant decrease in the concentration of 4-chlorophenol after 10 min of reaction was observed. The material in which the Ti precursor was added as sol (labeled as TSINS), presented the highest 4-chlorophenol degradation, reducing 86% of the initial concentration (2.33×10^{-4} mmol/cm^3). Liquid chromatography shows the formation of intermediate compounds resulting from the decomposition of 4-chlorophenol and their subsequent partial mineralization.

Keywords Monoliths · Photocatalytic degradation · 4-chlorophenol · Mineralization · Novel photocatalysts

1 Introduction

Nowadays, it is a common practice to use solid catalysts as small particles, fine powders or coatings, and activate them through several methods including those used in heterogeneous photocatalysis. The TiO_2 is by far, the material that exhibits the best photocatalytic properties as can be seen through a large number of works related with it [1, 2]. In addition to this, other TiO_2 systems doped with some metals such as Pt, Pd, Zn, Mo, W or supported on some materials such as activated carbon, have been reported [3–7]. However, an inconvenient for some of those materials is related to their limited capability of being recovered after the reaction is completed; mainly because those materials consist in small dispersed particles, many of them mixed with the treated effluent. This makes necessary to provide a separation stage that can be avoided by synthesizing the catalyst as structures (like monoliths) that do not flow away from the reaction system.

There is evidence that the synthesis conditions are fundamental to determine the final properties and catalytic characteristics of any catalytic system [8]. The porous materials have attracted the interest of researchers all around the globe due to their excellent physicochemical properties. Their relevance lies on their morphological and structural features that provide them high porosity and specific surface area values [9]. Some of those systems include silicon oxide and titanium oxide, which have

✉ Jaime Espino-Valencia
jespino@umich.mx

[1] Post Grad Division, Facultad de Ingeniería Química, Universidad Michoacana de San Nicolás de Hidalgo, Edificio V1, Ciudad Universitaria, Morelia, Michoacán 58060, México

[2] Chemical Eng. Lab., Centro Conjunto de Investigación en Química Sustentable, UAEM-UNAM, Universidad Autónoma del Estado de México, km 14.5 Toluca-Atlacomulco Road, San Cayetano, Piedras Blancas, Toluca, MEX 50200, México

[3] Instituto de Investigaciones Químico Biológicas, Universidad Michoacana de San Nicolás de Hidalgo, Edificio B2, Ciudad Universitaria, Morelia, Michoacán 58060, México

Published online: 02 July 2021

been studied in numerous applications. SiO_2 is very stable, exhibits high specific area values and excellent mechanical properties, however, it is inert in some reaction systems, which limits its application as catalyst [10]. Regarding the TiO_2, albeit being the most wide used photocatalyst, it is not thermally stable and its specific area is relatively low (30–50 m^2/g). In addition, specific surface area is strongly diminished when subjected to high temperatures; due to the transformation to several phases and crystal growth [11]. As a catalyst, it has shown the best photocatalytic activity and maximum performance, being observed that the properties that influence their activity are closely related to the specific surface area, crystallinity, crystal size and crystalline structure [12]. In general, the anatase phase is the most active allotropic form among the different available forms [13]. It has also been observed that the addition of oxides such as SiO_2 to its structure, can improve their thermal stability and photocatalytic activity [14].

Silica-titania materials have been developed in different ways: SiO_2-TiO_2 mixed oxides prepared by the sol–gel method combined with hydrothermal treatment [8], mesoporous coatings of SiO_2-TiO_2-P_2O_5 obtained by the sol–gel method combined with the EISA method [15], compounds in the form of silica-titania aerogels produced by chemical deposition of titanium in solution on a basis of silica nanoparticle [16]. Mesoporous silica-titania nanomaterials [17], thin TiO_2 films [18], to mention some of them. All for different applications showing that the method of preparation has a great influence on the physicochemical, morphological and structural properties.

Some other materials like TiO_2 modified with Co and Cr [19], TiO_2-mesh and TiO_2 P25 [20], sulphated Fe_2O_3-TiO_2 [21], Fe_3O_4-TiO_2-Ag nanocomposites [22] and Pt/TiO_2, Pd/TiO_2 catalysts [6], have been tested in the photocatalytic degradation or removal of organic pollutants such as 4-chlorophenol, which represents an important class of environmental pollutants in water, concluding that its photocatalytic efficiency could be associated with increases in the BET surface area, the particle size and adsorption effect of intermediate products, the temperature of calcination, the effect of composition and the influence of phases content, respectively. Many of these works only show the results of the decomposition of the 4-chlorophenol molecule, but do not present a complete analysis of the degradation. Furthermore, many catalysts are used in the form of powders, which could be disadvantageous and makes necessary to conduct studies from a different perspective, such as the analysis of by-products and their path to mineralization.

Currently, efforts continue to improve the catalytic activity of TiO_2 [23–25]. On this regard, the purpose of the present work is to show the characterization and photoactivity results of relatively new TiO_2-SiO_2 mesoporous materials obtained as monoliths, which can be applied to the treatment of wastewater, replacing traditional powder catalytic systems and thus solving the related problems such as the separation stage.

2 Material and methods

2.1 Catalyst synthesis

The materials were synthesized by the EISA method (Evaporation-Induced Self-Assembly) [26]. For the synthesis of the Si sol, Tetraethyl Ortho-Silicate [$C_8H_{20}O_4Si$, 98% Sigma Aldrich] (TEOS) was used as precursor of Si, nitric acid [HNO_3, 70%, Aldrich) as catalyst and ethanol [C_2H_6O, 99.5% Aldrich] as solvent at a molar ratio of 0.143:0.004:0.573, respectively. Titanium IV Butoxide [Ti (OC_4H_9)$_4$, 97%, Sigma Aldrich] as precursor of Ti and hexadecyl trimethyl ammonium $C_{19}H_{42}BrN$ bromide (CTAB) as surfactant, were used at a molar ratio of $1.75*10^{-2}$: $3.3*10^{-3}$, respectively. Finally, 4-chlorophenol [ClC_6H_4OH, 99%, Aldrich] was used as a model molecule for the study of the photocatalytic activity of materials synthetized.

To obtain the TiO_2-SiO_2 monoliths with 14 wt% of Ti, a Si sol was first prepared. For such a purpose, the ethanol was heated up to 60 °C under constant moderate stirring. Then, the CTAB surfactant was added and the mixture was stirred for 15 min. After this time the Tetraethyl Ortho-Silicate (TEOS) was added, and the stirring was kept for further 15 min. Finally, a hydrolysis solution (deionized water and nitric acid with at a molar ratio 3.33:0.004, respectively) was dropwise added, stirring the system for one hour.

Once the Si sol was prepared, the titanium IV butoxide was added by two different ways: a) directly into the Si sol before gelation and, b) as a Ti sol (mixing titanium butoxide IV, ethanol and nitric acid at a molar ratio $5.94*10^{-2}$:$8.89*10^{-2}$:$2.58*10^{-2}$, respectively) into the Si sol. This resulted in a colloidal dispersion that allows the direct interaction of the Ti with the Si species during the sol–gel process. After two hours of stirring under moderate constant speed, 2.5 cm^3 to 3 cm^3 aliquots were taken from the resulting mixture and placed in plastic containers, keeping this in a slow drying chamber at room temperature, until the monoliths formation was completed. During the process, which was carried out in an acidic medium, all the hydrolysis and condensation reactions were completed. In this process, the tetraethylortosilicate reacts with water molecules forming siloxane groups which in turn, together with the Ti molecules could form Si–O-Ti bonds, as described by the following reactions sequence [27],

$$\text{Hydrolysis}: \quad Si{-}O{-}C_2H_5 + H_2O = Si{-}OH + C_2H_5OH \tag{1}$$

$$\text{Condensation}: \ \mathrm{Si-O-C_2H_5 + Si-OH} = \mathrm{Si-O-Si + C_2H_5OH} \quad (2)$$

$$\mathrm{Si-OH + Si-OH = Si-O-Si + H_2O}$$

$$\text{Condensation}: \ \mathrm{Ti-O-C_4H_9 + Si-OH} = \mathrm{Si-O-Ti + C_4H_9OH} \quad (3)$$

After the monoliths were formed, some of them were calcined at 600 °C under air flow, at 1 °C/min using two heating stages (from room temperature to 125 °C, for 3 h and from 125 °C to 600 °C for 2 h), and other portion of monoliths were calcined without air flow at the same conditions. This moderate ramp allows the orderly release of the organic phase, preventing the structure from collapsing during the process. The materials were labeled as TSIN in the case of the direct addition of the Ti precursor to the Si sol and TSINS in the case of the Ti sol addition to the Si sol; both calcined without air flow. Similarly, TSINF/A and TSINSF/A are the tags given to those compounds that were calcined under air flow.

2.2 Catalysts characterization

The samples were characterized using an X-ray diffractometer (XRD), model D8 ADVANCE DAVINCI. This allowed the analysis of the crystalline structure of the materials. The patterns were obtained using CuK radiation, a voltage of 30 kV and current of 20 mA. The difractograms were scanned at 2θ angles from 10° to 90° with 2°/min steps.

The pore size distribution and specific surface areas were analyzed using an Autosorb iQ Quantachrome Nitrogen Adsorption equipment. Adsorption–desorption isotherms were obtained using liquid nitrogen at -196 °C. The materials were out-gassed at 250 °C for 2.5 h. The specific surface areas of the materials were calculated by BET (Brunauer–Emmett–Teller) method and pore size distribution by BJH (Barret-Joyner-Halenda) method.

Thermogravimetric (TGA) analysis and differential scanning calorimetry (DSC) diagrams were obtained using a thermogravimetric equipment Perkin Elmer model STA 6000, using nitrogen gas at 22 cm^3/min, 19.169 g of material and heating from 25 °C to 800 °C at 1 °C/min. The particle size and morphological properties were analyzed using a JEOL Scanning Electron Microscope (SEM) of field emission; model JSM 7600F and a Transmission Electron Microscope (TEM) JEOL-2100 model at 100 kV. Also, the materials were analyzed by Infrared Spectroscopy using a Shimadzu IR Trace-100 Fourier IR spectrometer (FT-IR), Japan, and using attenuated total reflectance (ATR). This was conducted at room temperature, with 12 scans, a resolution of 4 cm^{-1}, and a wave number range of 4000–500 cm^{-1}.

2.3 Photocatalytic activity

The photocatalytic activity of the materials was tested using a 150 cm^3 glass batch cylindrical reactor with a diameter of 4.5 cm, provided with magnetic stirring, oxygen flow (air) and a refrigerant to control the system temperature. UV lamp (Pen Ray 8 W) of 5.4 cm in length, 0.6 cm in diameter and a wavelength of 254 nm was used as a source of ultraviolet radiation. A portion of the monolith, about of 8×10^{-4} g/cm^3 was used as catalyst. This catalyst concentration was previously selected from studies with materials of TiO_2 in order to determine the optimum loading for our conditions and has previously been reported [12]. In addition, it has been observed that the initial photodegradation rate rapidly increases with catalyst loading up to 1×10^{-3} g/cm^3. Also, at high catalyst concentration light scattering and screening effects are are observed, reducing the absorption of photons and consequently the degradation rate [20]. The model molecule to be degraded was 4-chlorophenol in aqueous solution with an initial concentration of 2.33×10^{-4} mmol/cm^3. Lower concentrations were not tested because the 4-CP oxidation was that fast in the first minutes of reaction that the measurement of degradation rate was not feasible. The reaction was carried out in acidic medium (pH = 4), under moderate constant stirring and room temperature. This pH value was considered based on some reports [28, 29], in which it is mentioned that the TiO_2 surface has a positive charge at low pH values, while chlorophenols have negative and neutral charges at those same pH values, facilitating the adsorption of the organic molecule which promotes photocatalytic degradation. In the case of temperature, Rideh et al. [30] affirm that the oxidation of 4-chlorophenol is not affected in the range of 25–65 °C, which gives opportunity to work the system under normal conditions, reducing operating costs. The reaction time was one hour and aliquots (1cm^3 samples) were taken every 10 min to be analyzed.

2.4 Chemical analysis

The reaction progress was verified as a function of time. The removal of 4-chlorophenol and determination of intermediary products; including aromatic compounds and carboxylic acids, was performed in a UHPLC Vanquish Thermoscientific equipment. The mobile phase used was a 5 mM sulfuric acid–methanol solution in an 80:20 (v/v) ratio with a 1 cm^3/min flow. The chromatographic column was an Ascentis Express C-18 (Supelco). For the quantification of the analyzed samples, a calibration curve was prepared for each

of the studied by-products using 6 standard solutions with concentrations between 1×10^{-6} g/cm^3 and 5×10^{-5} g/cm^3.

For the determination of carboxylic acids, a mixture of 970 cm^3 of monobasic potassium phosphate buffer (1.2 g in 1000 3cm^3 of water) and 30 cm^3 of methanol was used as mobile phase (solution A) and HPLC grade methanol as a solution B, the proportion was 96.5% of solution A and 3.5% of solution B at a flow rate of 0.5 ^{cm3}/min. The column used for the separation of the compounds was an Eclipse XDB C-18 brand Zorbax, 15 cm in length and 4.6 mm in diameter. A calibration curve was prepared for each of the compounds with 6 standard solutions with concentrations between 5×10^{-6} g/cm^3 and 1×10^{-4} g/cm^3 from two stock solutions for each compound.

The mineralization extent of 4-chlorophenol, at the end of the reaction, was determined by using a TOC-L, Shimadzu equipment that allows the quantification of total organic carbon.

3 Results and discussion

TiO_2-SiO_2 monoliths with different physical appearance were obtained, which is due to the way to add the Ti precursor, as was described in the Sect. 2 (catalysts syntehesis). In the first case, where the titanium IV butoxide was added directly into the Si sol before gel formation (TSIN), opaque materials were obtained (Fig. 1a); while in the second case, when the titanium IV butoxide was added as a sol (TSINS), materials completely transparent were formed (Fig. 1b). These transparent materials may be better for photocatalytic applications by easing the penetration and absorption of UV light in the catalyst. In both cases, the prepared materials were monolith discs with diameters between 0.9 and 1.2 cm and 2 mm of thickness. This geometry allows the synthesized materials to be used either in a packed bed or as slurry after grinding and sieving them.

3.1 Materials characterization

3.1.1 Nitrogen physisorption

All materials were characterized by nitrogen physisorption. The specific surface area and average pore size values obtained by this technique are summarized in Table 1. According to these results, there is an important effect of the synthesis and heat treatment conditions on the textural properties. Those materials where the Ti precursor was directly added, present a greater variation of specific surface area and average pore diameter, which may be related to a greater interaction between Si and Ti during the drying and heat treatment process, causing rearrangement of species. In

Table 1 Specific surface area and pore size distribution of the materials; with direct addition of the Ti precursor to the Si sol (TSIN) and with addition of the Ti sol to the Si sol (TSINS), calcined without and with air flow (F/A), respectively

Sample	Specific surface area (m^2/g)	Average pore size (nm)	Average pore volume (cc/g)
TSIN	527.9	3.8	0.75
TSIN F/A	813.8	4.9	0.90
TSINS	756.4	3.4	0.17
TSINS F/A	788	3.1	0.27

Fig. 1 Monoliths of TiO_2-SiO_2: **a**) With direct addition of the Ti precursor to the Ti sol (TSIN); **b**) With addition of the Ti sol to the Si sol (TSINS)

general, high surface area values can be observed, greater than 800 m^2/g in the case of TSIN material. These values are even greater than some SiO_2 materials obtained by the traditional sol–gel method, with typical values between 200 m^2/g and 700 m^2/g [31, 32]. These results are interesting to highlight that through the EISA method during the preparation of Si sol, the active phase can be deposited without sacrificing the value of the exposed surface area, which would not happen with some other methods, such as impregnation for example, where is expected that the deposition of active phases decreases the specific surface area, because they obstruct the pores of the support.

In the pore size distribution (Fig. 2), it is observed that all the materials show pore diameters in the range of mesoporous materials according to the IUPAC classification. The highest pore volume values were presented by those materials in which the Ti precursor was directly added. It is probably due to the possible segregation of Ti species producing a structural rearrangement, generating empty spaces and therefore increasing the pore volume of the system.

The air flow during the calcination also affects the final properties of the material. These characteristics depend on the arrangement of the species within the structure of the monolith. In this particular case, both materials, TSIN and TSINS, are benefited when they are calcined under air flow, observing an increase in the value of the surface area associated with an increase in pore volume. This is because during this process, the rearrangement of the species occurs in a more orderly way, even though the organic component and the volatile compounds are forced to leave at a greater speed. This prevents the collapse of the structure momentarily occupying the space taken by the released species. These properties may influence the catalytic activity by altering the diffusion of the species through the pores during the reaction process.

The resulting adsorption–desorption isotherms are of type IV. These isotherms are characteristic of mesoporous materials and so is the shape of the hysteresis of the triangular type H2 produced by the synthesis method used [32]. The TSINS material calcined under air flow shows higher adsorption volumes. This coincides with the pore volume values, which is also higher. In the case of the TSIN material (calcined under air flow), it exhibits lower adsorption volumes at low relative pressures, however, for values greater than 0.8 (relative pressures) the volumes are greater than TSIN calcined without air flow. This could be due to structural rearrangement, increased pore volume and diameter enlargement.

3.1.2 X-ray diffraction characterization

The X-ray diffraction patterns for thermally treated materials with air flow (Fig. 3) show a structural arrangement when the Ti precursor was added directly, where the crystalline phases corresponding to the anatase phase can be observed at angle 2θ next to 36, 44.1, 54.3, and 63.4 corresponding to the (103), (004), (105), and (204) planes, respectively. The differences observed at 27.5, 41.2, 56.6 and 69.25, corresponding to (110), (111), (220) and (301) planes, respectively, referred as rutile phases [1, 33]. It is important to mention that the TiO_2-SiO_2 materials did not show the diffraction peaks corresponding to planes (101) and (200) of anatase phase that normally appear in TiO_2 materials. This fact suggests the restructuring of the material during the heat treatment process, in which the titanium

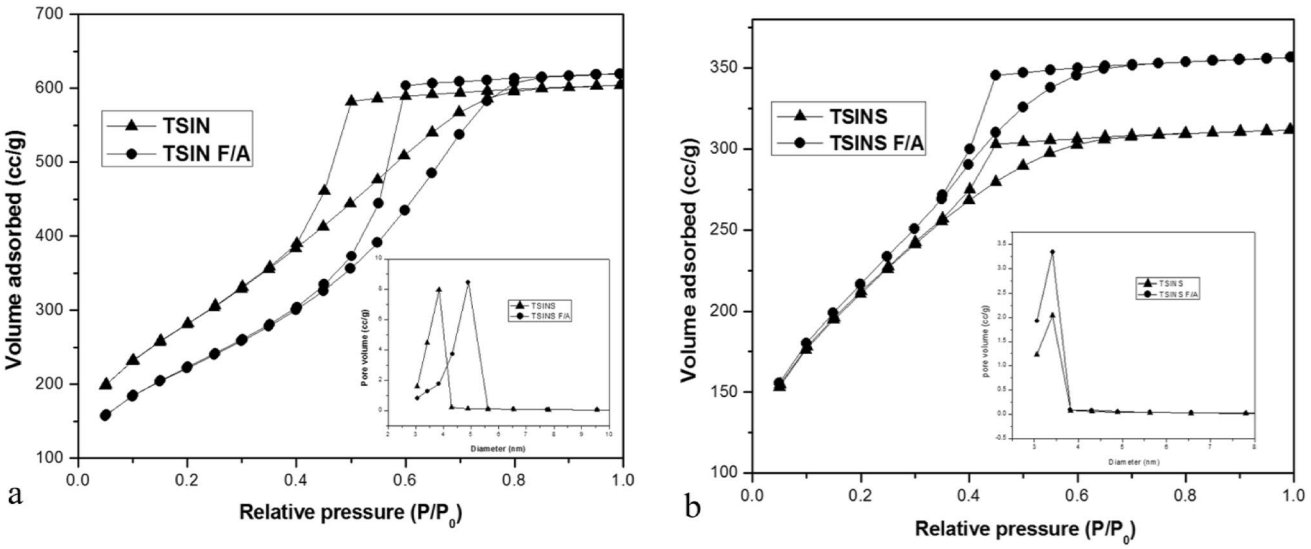

Fig. 2 N_2 adsorption–desorption isotherms and pore size distribution: **a**) TSIN; **b**) TSINS: -▲- calcined without air flow, -●- calcined under air flow

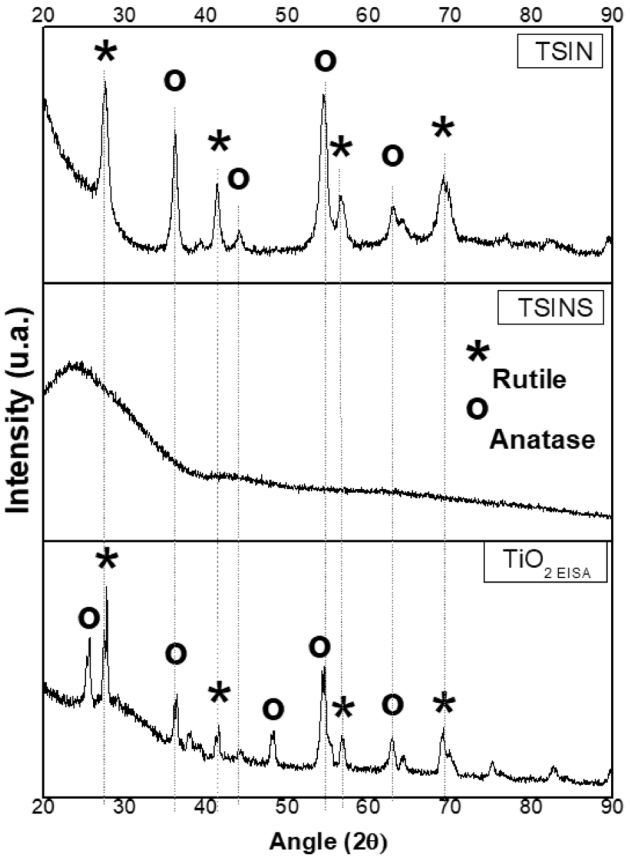

Fig. 3 XRD patterns of the materials calcined under air flow

species tend to orient themselves in the other directions. In the case of materials where the Ti precursor was added as a sol, an amorphous structure is observed, showing only the characteristic band that corresponds to SiO_2. In this case, it is possible to assume that during the synthesis process the presence of the solvent, and specifically, the influence of the catalyst could strongly contribute to homogeneous distribution of the active phase, avoiding precipitation of the Ti or formation of anatase and rutile phases. This can lead to the possible formation of a greater number of structures with Ti–O-Si bonds, keeping the Ti species distributed into the silica matrix. This may explain the observed white or opaque structures in the first case, and transparent structures in the second case. Finally, it is important to mention that no significant difference in the diffraction patterns was observed for the materials calcined without air flow.

3.1.3 FT-IR analysis

Figure 4 shows the results of the IR analysis. The TSIN materials show a decrease of the transmittance between 1000–500 cm^{-1} which is characteristic of the TiO_2 anatase phase (Fig. 4a). Some vibrational bands between 2000–1200 cm^{-1} may be related to the polymerization of Si-0H groups forming Si–O-Si bonds [34]. According to Amlouk et al. [35], the vibrational bands in the interval of 1070–1098 cm^{-1} and 790-806 cm^{-1} correspond to the asymmetric and symmetric stretching, respectively, of the Si–O-Si bond, which coincides with the TSINS materials (Fig. 4b). The vibration band in the 947–967 cm^{-1} interval, for this same material, is attributed to the elongation vibration of the Si–O-Ti bond [36]. This could demonstrate the interaction between silica and titania. The band attributed to the symmetric elongation of Ti–O-Ti was not observed in our results.

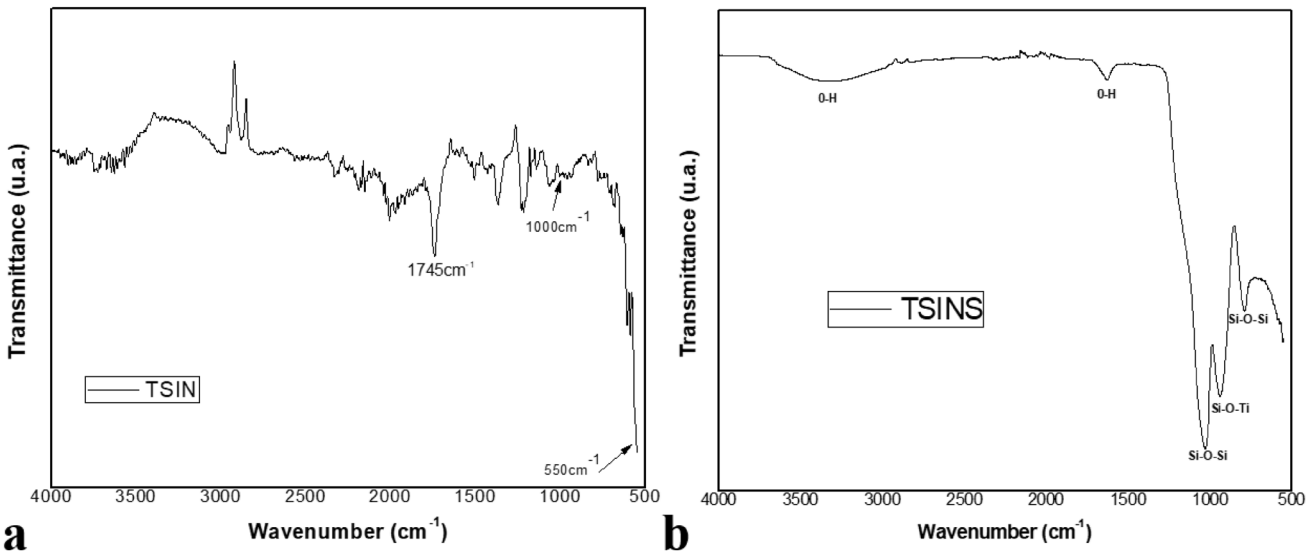

Fig. 4 IR spectrum: **a**) with direct addition to the Ti precursor; **b**) with addition of the precursor as a sol

3.1.4 SEM and TEM analysis

Figure 5 shows images obtained by Scanning Electron Microscopy analysis for materials with the best surface area property. In the materials where the active phase was directly added (TSIN), the presence of exposed material on the surface can be observed (Fig. 5a; Fig. 5b). According to the XRD results, these could be titanium particles exposed on the surface, they have a particle size, according to the micrographs, between 80 and 100 nm. These values are similar to the commercial material Degussa P25, which is constituted by particles up to 85 nm for the anatase phase [37]. The micrographs for the material in which the Ti precursor was added as a sol (TSINS), homogeneous structures are observed and without surface defects, with some particles of approximately 1.21 µm standing out (Fig. 5c; Fig. 5d). It should be mentioned that the monoliths of TiO_2-SiO_2 in both cases do not present cracks or discontinuity on the surface. Thus, it can be inferred that the synthesized materials are thermally and mechanically stable.

Results of the analysis by transmission electron microscopy show that the materials TSIN, in which the Ti precursor was directly added to the Si sol (Fig. 6), present structures with local or point crystal growths, its shape is similar to a bun formed by phases that extend in different directions with lengths ranging between 0.41 and 0.49 nm. Thus, it can be assumed that the center was the promoter for the growth of said particles during the heat treatment, which is where the characteristic phases of titania could have been formed. It is important to mention that it seems that not all forms have finished developing, since some are more spherical than others. On the other hand, in the case of the materials TSNIS, in which the Ti was added as a sol (Fig. 7), these exhibit the formation of crystalline phases, very common in this

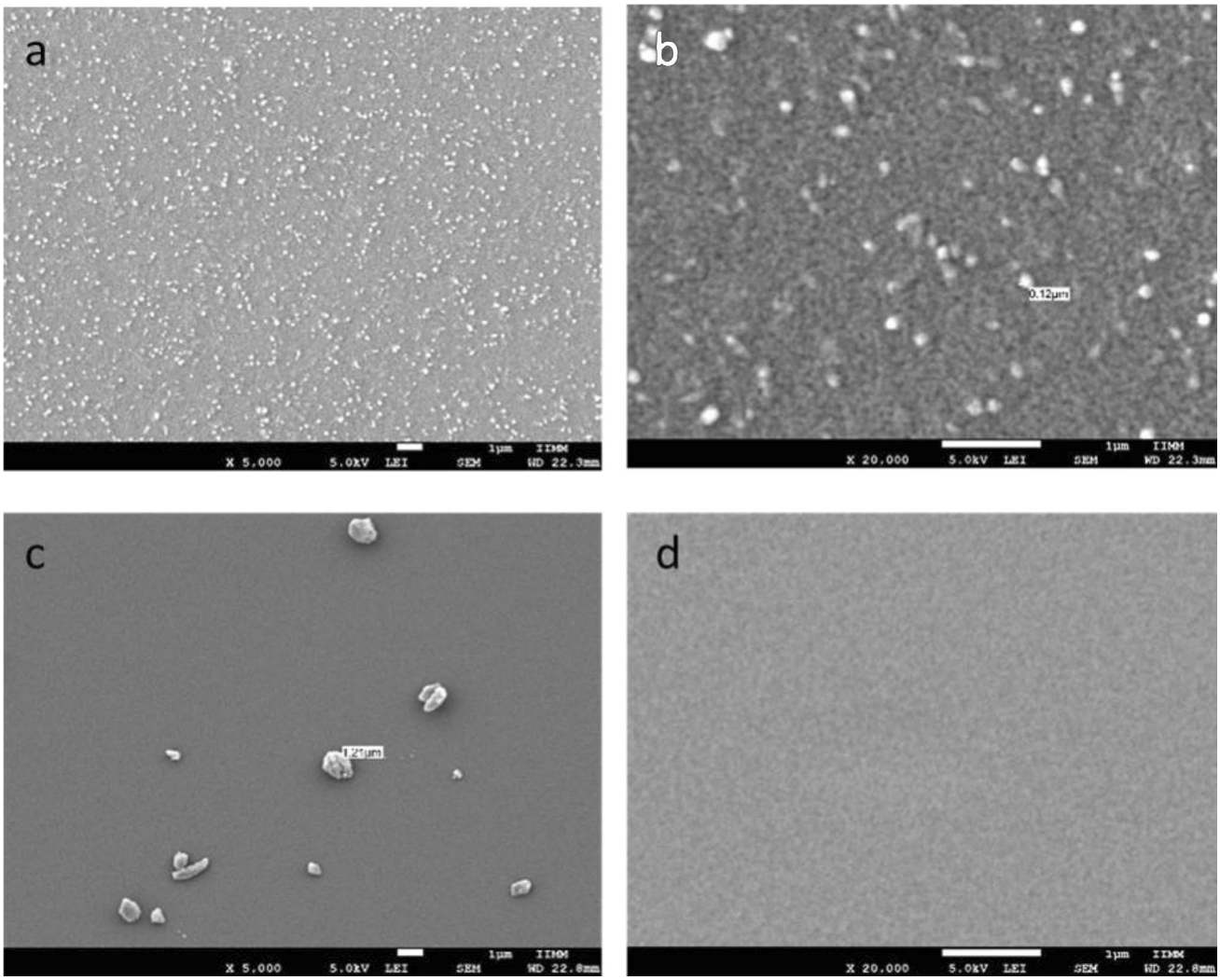

Fig. 5 SEM Images of synthesized compound at 5000x and 20000x: (**a** and **b**) with direct addition of the Ti precursor, (**c** and **d**) with addition of the Ti precursor as a sol

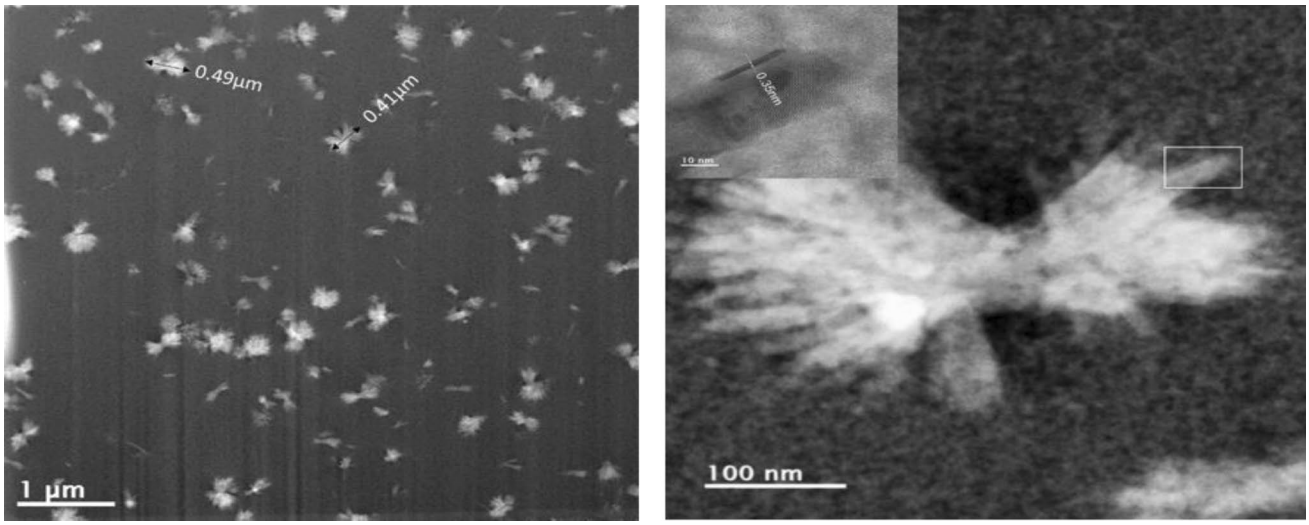

Fig. 6 TEM Images of materials obtained with direct addition of the precursor (TSIN)

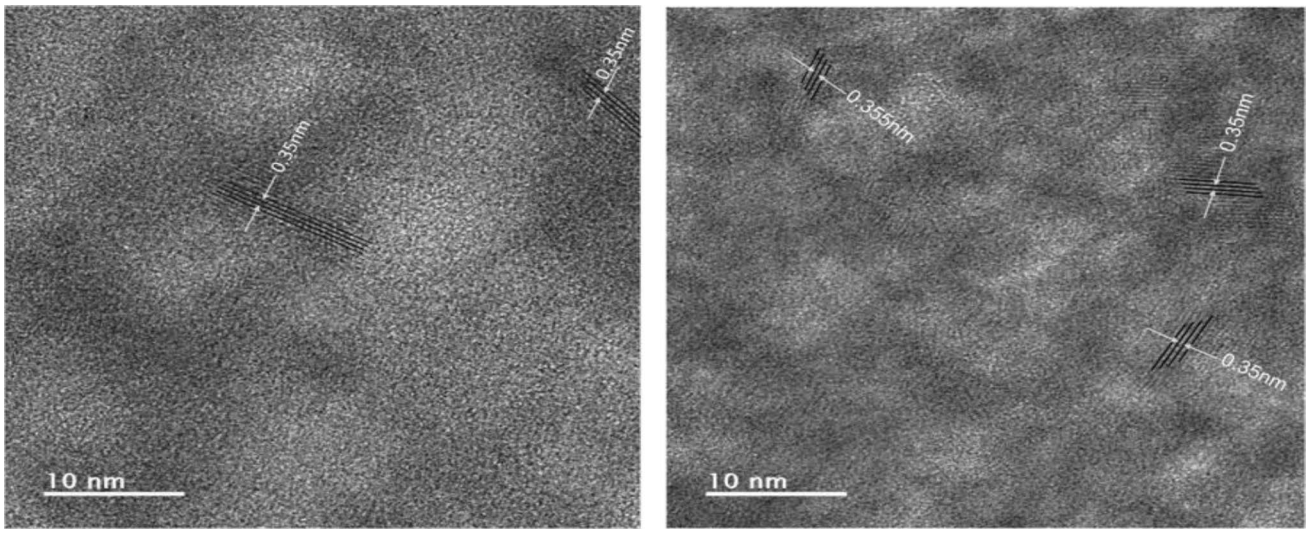

Fig. 7 HRTEM Images of materials obtained with addition of the Ti precursor as sol (TSINS)

type of materials, with crystal sizes corresponding to the anatase phase, oriented in the plane (101) [7, 38], with an interatomic space of 0.35 nm.

3.1.5 DSC and TGA analysis

Results of the TGA analysis using nitrogen flow for the TSIN and TSINS samples (Fig. 8) show that for both materials, the greatest weight loss is observed during the first stage of the heat treatment, from 25 °C to 125 °C in an approximate time of 20 min. At this stage, much of the unreacted reagents with relatively low boiling point such as water and ethanol are eliminated. TSINS materials show a weight loss of approximately 18 wt% while the weight loss in the TSIN monoliths was only of 10 wt%. This difference is associated with the amount of solvent used during the synthesis process; in the first case it was greater than in the second. In the second stage of heat treatment, from 125 °C to 600 °C, where a more severe structural rearrangement can occur and in which the organic phase used to model the structure of the material is completely released, a constant behavior is observed in the weight loss for the TSINS material up to 24%, due to the characteristics of the thermogram. This material shows a good thermal stability during the heat treatment process.

In the case of the TSIN material, this shows a first weight loss between 25 °C and 120 °C, which can be due to the desorption of physically adsorbed water molecules, then a second weight loss at 225 °C, which has been

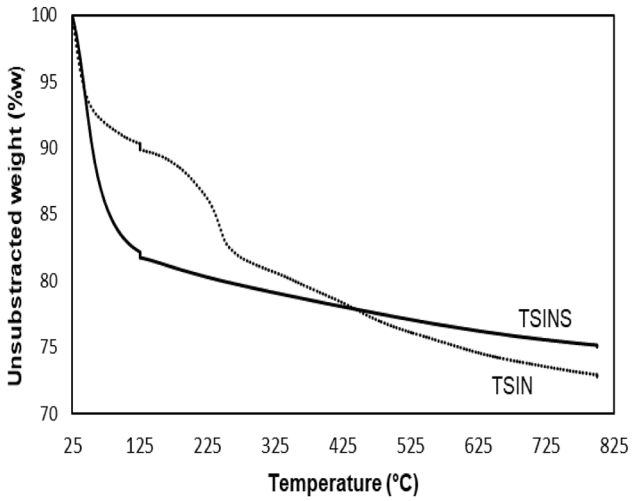

Fig. 8 TGA diagrams: ●●●●● materials with direct addition of the Ti precursor, — materials with addition of the Ti precursor as a sol

attributed to the removal of absorbed hydroxyl groups and surface water molecules [21] and finally a third weight loss at the end of the heat treatment process up to 27%. This behavior could be attributable to a significant restructuring that allows the organic phase to exit faster, according to the X-ray diffraction patterns. In this step is where the ordering of species might occur, forming the characteristic patterns. Regarding the DSC analysis (Fig. 9), the results do not show endothermic or exothermic peaks. This suggests that the synthesized materials do not present changes or transitions of spontaneous phase during the heat treatment process.

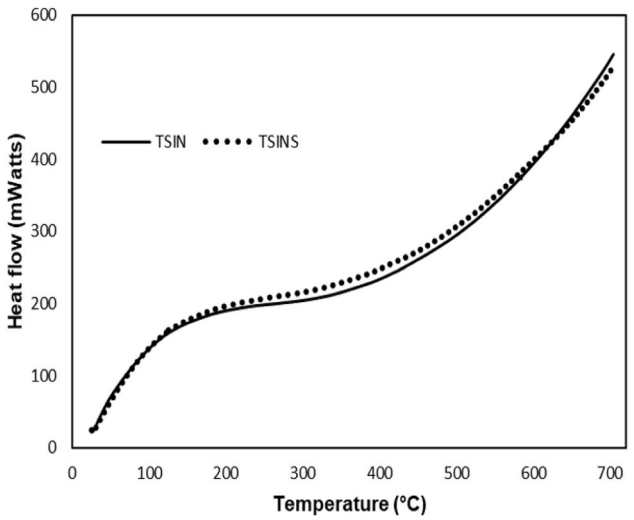

Fig. 9 DSC diagrams: — materials with direct addition of the Ti precursor, ●●●●● materials with addition of the Ti precursor as a sol

3.2 Photocatalytic activity

The removal of 4-chlorophenol by photolysis and adsorption was first analyzed (Fig. 10). The effect of photolysis was studied by carrying out the experiment only in the presence of oxygen and UV light without catalytic material. The degradation of 4-chlorophenol by direct photolysis is negligible and the apparent increase in the concentration in the first 30 min is due to an electronic effect that modifies the UV absorbance spectrum of the solution and appears as if it was an increase in concentration [39]. Therefore, this increase is not attributed to the reagents. This phenomenon is described as a period of photoinduction associated with the formation of free radicals [40, 41], whose effect is negligible considering the low free radical concentration and their molar absorption coefficient compared to the select pollutants. After 30 min no significant changes were observed with respect to the initial concentration.

Regarding the removal of 4-chlorophenol by adsorption, it was observed that a 9% was removed by this means by the TSIN material. This effect could be attributable to chemisorption produced by the Ti species exposed on the surface that do not need to be photoexcited, as can be seen in the scanning electron microscopy micrographs (Fig. 5). With the TSINS (addition of the Ti precursor as a sol) material, no significant changes were observed with respect to the initial concentration of the reagent.

To observe the synergism between the Ti and Si species, in the TiO_2-SiO_2 monoliths, it was necessary to study the individual behavior of the species under the same reaction conditions. For that purpose, Si and Ti monoliths

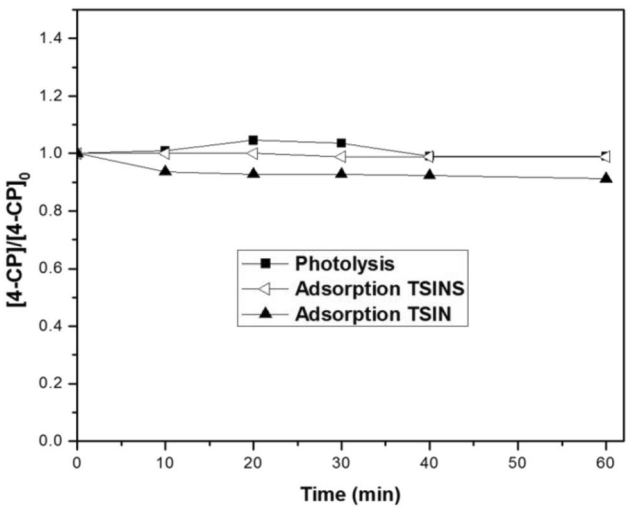

Fig. 10 Photolysis and adsorption, -■- Photolysis, -▲- materials with direct addition of the Ti precursor, -●- materials with addition of the Ti precursor as a sol. Reaction conditions: room temperature, Initial concentration = 2.33×10^{-4} mmol/cm^3, catalyst loading = 8×10^{-4} g/cm^3

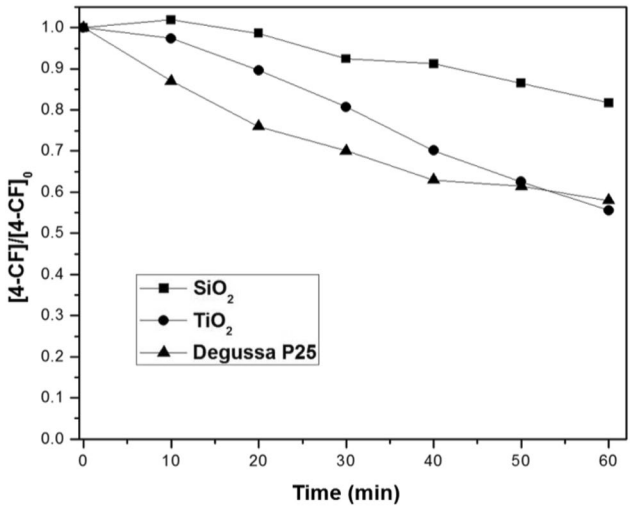

Fig. 11 Photocatalytic activity of monoliths TiO_2, SiO_2 and Degussa P25 material. Reaction conditions: room temperature, Initial concentration = 2.33×10^{-4} mmol/cm^3, catalyst loading = 8×10^{-4} g/cm^3

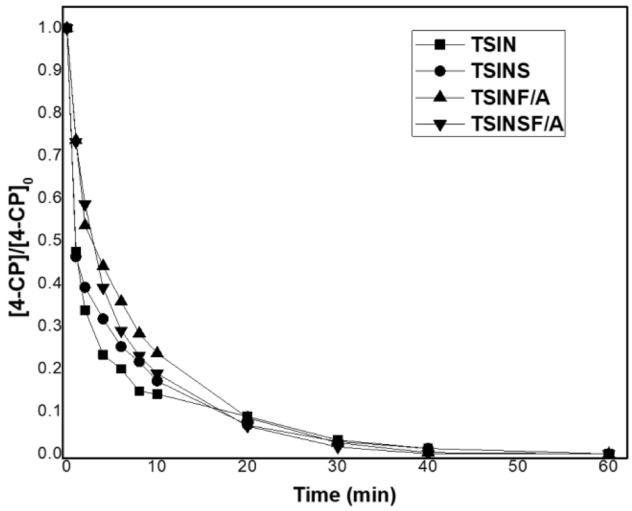

Fig. 12 Photocatalytic Activity of monoliths TiO_2-SiO_2 analyzed by HPLC. Reaction conditions: room temperature, initial concentration = 2.33×10^{-4} mmol/cm^3, catalyst loading = 8×10^{-4} g/cm^3

were prepared separately by the EISA method and tested in the degradation of 4-chlorophenol. For comparison purposes, an experiment was also conducted with the commercial catalyst Degussa P25 and the results are shown in Fig. 11. It can be observed in Fig. 11, that the Si monoliths removed about 19% of 4-chlorophenol after 60 min of irradiation. According to Arai et al. [42], silica has a pH value at the isoelectric point of 2.25, for this reason, at pH values of 3.0–4.0 the surface is negatively charged preventing a large number of pollutant molecules such as chlorophenols from adsorbing. Even though it is known that silica is an inert material, the adsorption of species on the surface and some hydroxyl groups that in presence of ultraviolet light act as oxidizing species, could explain the removal of 4-chlorophenol [31]. The Ti monoliths and the commercial material known as Degussa P25, tested under the same reaction conditions, showed a very similar removal percentage of 4-chlorophenol, about 45% and 42%, respectively, after 60 min of reaction.

The results of the photocatalytic activity for TiO_2-SiO_2 monoliths are shown in Fig. 12. To quantify the species participating in the removal process, the reaction solution at different times was analyzed by liquids chromatography (HPLC). In general, an important decrease in the concentration of 4-chlorophenol in the first 10 min of reaction was observed at all cases, this effect in the degradation rate can be associated to the loading of the TiO_2-SiO_2 material, favoring the increase of hydroxyl radical generation on the catalyst surface. After this time the removal process is slower, however only 50 min are necessary to have a complete removal of the reagent.

The behavior of the materials reveals the importance of the effect caused by the interaction between Si and Ti species in the catalytic activity. The species together in the monoliths Si-Ti are more active than the same separately, this effect can be observed, when comparing the degradation profiles (Fig. 11 with Fig. 12), it seems that there is an addition of the catalytic activity of the species. The photocatalytic efficiency of the materials synthesized could be related with their improved characteristics. The combination of Ti and Si species results in materials with high specific surface area, favoring the adsorption capacity toward molecules such as 4-chlorophenol. In addition, the diameter and pore volume values are parameters associated with the observed photocatalytic behavior. The form of incorporation of the precursors is another factor that improves the photocatalytic efficiency, with the employed preparation method, materials with TiO_2-SiO_2 species not only on the surface, also inside its structure, can be formed. The Si sol is an excellent dispersal medium for Ti species, not forgetting the addition route of the Ti precursor. Furthermore, when Ti is added as a sol, the solvent and the catalyst help to disperse the species in the Si sol.

The photocatalytic mechanisms can be summarized as follows: the solid is illuminated and due to the low pH of the solution, the sites are activated forming hole-electron pairs. These holes escape from the direct inner reaching the surface of the material and reacting with hydroxyl groups or adsorbed water to produce •OH radicals. The adsorptive dioxygen traps the conduction band electrons to form superoxide radical anions (O^2•−), followed by the generation of H_2O_2 and finally the formation of •OH radicals [38]. All this causing the solids surface to tend to a positive charge, while

chlorophenols have negative and neutral charges [28], facilitating the adsorption of the organic molecule which promotes photocatalytic degradation, forming hydroxyl groups capable of attacking and oxidizing the organic species present to form intermediaries and subsequent end products.

Materials calcined without air flow have a higher initial reaction rate (1.96×10^{-2} g/g_{cat}*min and 2×10^{-2} g/g_{cat}*min for TSINS and TSIN respectively), than those that were treated under air flow (9.87×10^{-3} g/g_{cat}*min and 1×10^{-2} g/g_{cat}*min for TSINSF/A and TSINF/A respectively), these values are even greater than some systems modified with molybdenum and tungsten (Avilés-garcía et al., 2017), thus favoring the percentage of removal of 4-chlorophenol in the first 10 min, 86% in the case of the TSINS material and 83% in the case of the TSIN material.

The decomposition of the 4-chlorophenol involves the formation of intermediate species and their possible mineralization to CO_2 and H_2O [7, 22]. The results of the UHPLC analysis of the reactions with the four solids (Figs. 13, 14, 15, 16) show that during the first 10 min of reaction, which is the time in which the greater amount of 4-chlorophenol is removed, intermediaries such as 4-chlorocatechol, hydroquinone and some traces of phenol were obtained, also appearing some acids such as: oxalic, formic, malonic, maleic, acetic and succinic. In this time interval no mineralization of any of the species is observed, that is, no degradation of any of the mentioned sub-products is observed. However, according to the plotted profiles, it seems that at higher reaction times, in all cases, the decomposition of organic species occurs and a large amount of succinic, oxalic and malonic acid appears. A complete mineralization begins after 30 min and 65% is reached in the case of opaque-looking materials, in which the Ti precursor was directly added (TSIN and TSIN F/A).

Table 2 shows the results of the analysis of Total Organic Carbon (TOC), to the end of the 4-chlorophenol degradation process, with the different materials. Those in which the Ti precursor was added directly to the Si sol (TSIN) showed a high percentage of mineralization of the intermediate products (more than 80%). This behavior could be associated with the adsorption–desorption capacity of the materials (Fig. 2), which allows both 4-chlorophenol and intermediate products to be adsorbed on the catalyst surface and interact with free electrons and OH groups, breaking the molecules until they are degraded to CO_2 and water. According to Fig. 17 these same materials are the ones that presented the highest initial mineralization speed. Otherwise, the materials in which the Ti precursor was added in solution to the Si sol showed a lower percentage of mineralization, being that the material calcined under air flow (TSINSF/A) only showed around 10% mineralization. In Fig. 18, the percentage of total organic carbon remaining at the end of the reaction is shown, in the case of removal using the TSINSF/A catalyst,

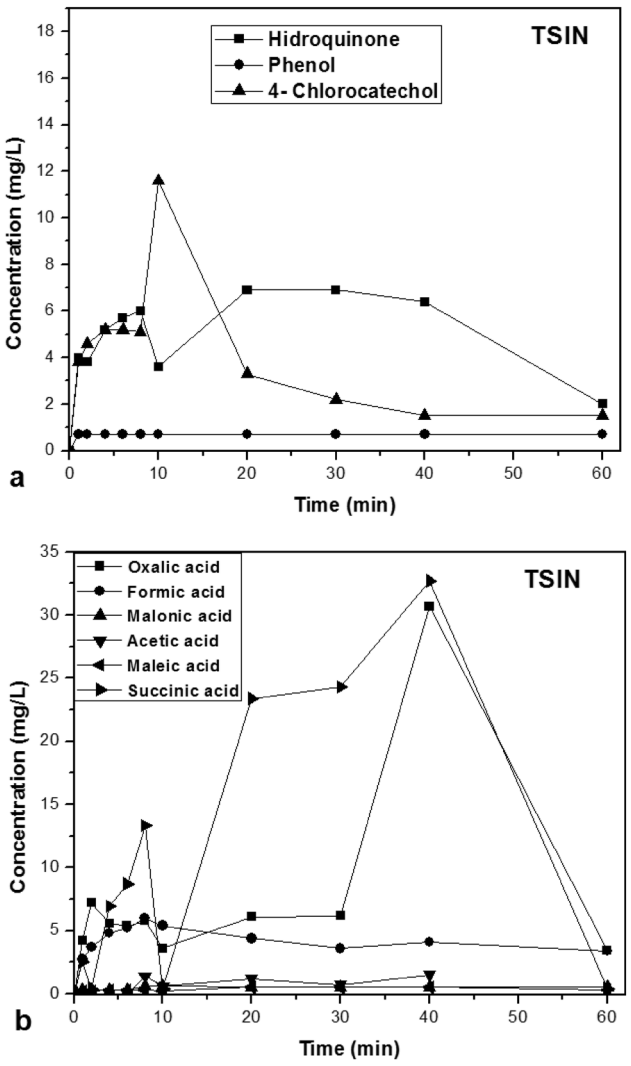

Fig. 13 Distribution of products obtained during the 4-chlorophenol oxidation when using TiO_2-SiO_2 monoliths prepared with the direct addition of the Ti precursor

large amounts of succinic acid were observed at the end of the process.

For the kinetic study of the reaction, the Langmuir–Hinshelwood model was applied, this is one of the most used models to represent the degradation kinetics of phenolic compounds by photocatalysis in aqueous medium [6, 43, 44]. This model is especially useful when intermediate compounds appear, products of oxidation, which accumulate on the surface of the catalyst, due to an adsorption effect. Table 3 shows the values of the equilibrium adsorption constant on the surface of the $K_{4\text{-CF}}$ catalyst and the reaction kinetic constant, K_a. These were calculated by linearizing the mentioned model, plotting $1/-r_a$ vs $1/C_{4\text{-CF}}$ and conducting a linear regression, observing a good adjustment of the experimental data to a first order behavior. According to the values of K_a, the materials that present a better activity are

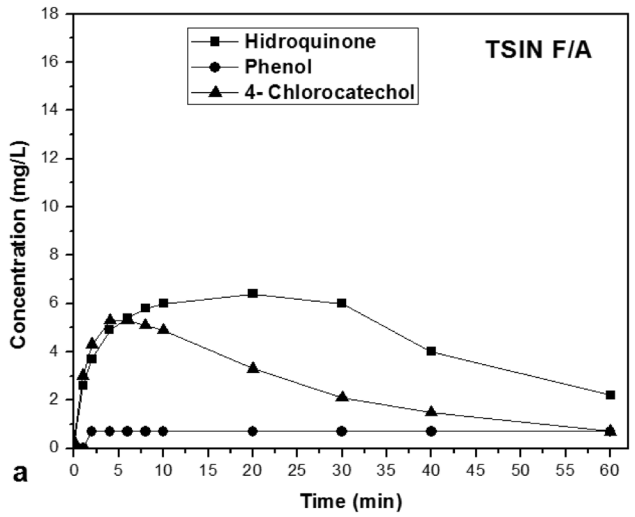

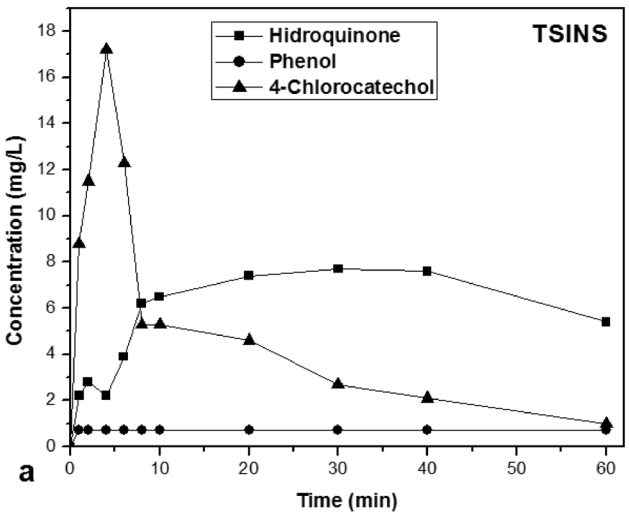

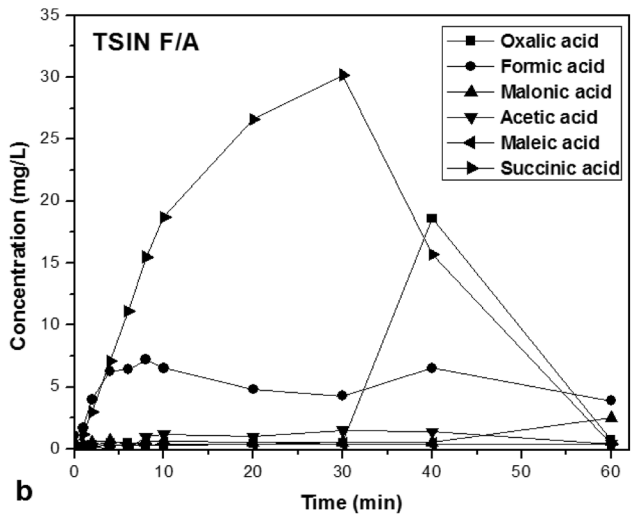

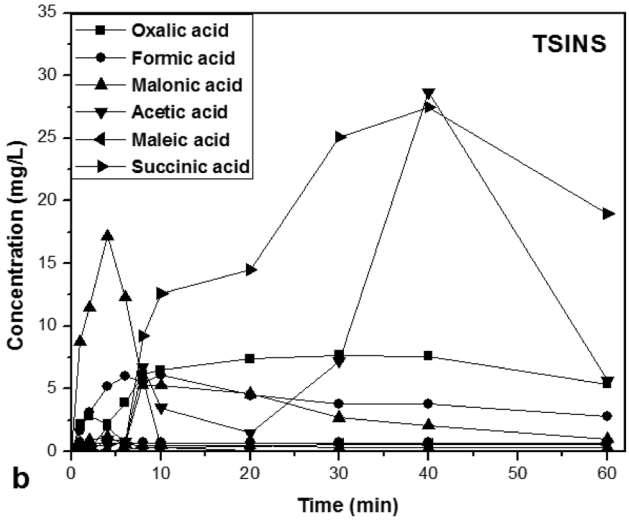

Fig. 14 Effect of air flow during calcination on the 4-Chlorophenol oxidation product distribution when using TiO_2-SiO_2 monoliths prepared with direct addition of the Ti precursor

Fig. 15 Distribution of products obtained during the of 4-chlorophenol oxidation when using TiO_2-SiO_2 monoliths prepared with the addition of the Ti as a sol

those of TiO_2-SiO_2 calcined under air flow and those of TiO_2 EISA, with values of $2.08*10^{-6}$ and $1.96*10^{-6}$, respectively. These values are higher than those reported by Theurich et al. [45] for the reaction in aqueous 4-chlorophenol solution catalyzed with titanium dioxide. At this point is worth bearing on mind that the reaction conditions were also different so a direct comparison should be taken with caution.

4 Conclusions

Using the EISA method, it is possible to produce TiO_2-SiO_2 monoliths, with photoactive phases dispersed on the Si, without negatively affecting properties such as surface area, which would not occur with some other methods, such as impregnation. The form of adding the Ti precursor has an important effect on the final textural, morphological and structural properties of the monoliths. The IR results showed a synergistic effect caused by the interaction between the Si and Ti species forming Si–O-Ti bonds. A great percentage of removal of 4-chlorophenol in just 10 min (greater than 80%) of reaction was observed, unlike when using only SiO_2 or TiO_2 monoliths. In all tested materials, the decomposition of organic species occurs and a large amount of succinic, oxalic and malonic acid appears. An important mineralization process was observed after 30 min, reaching around 88% in the case of opaque-looking materials, in which the Ti precursor was directly added. The use of monolithic materials in photoreactions solves the problem of powders that remain suspended after the reaction processes and have the potential to be used in packed bed photocatalytic reactors not only to carry out complete oxidation reactions but also partial.

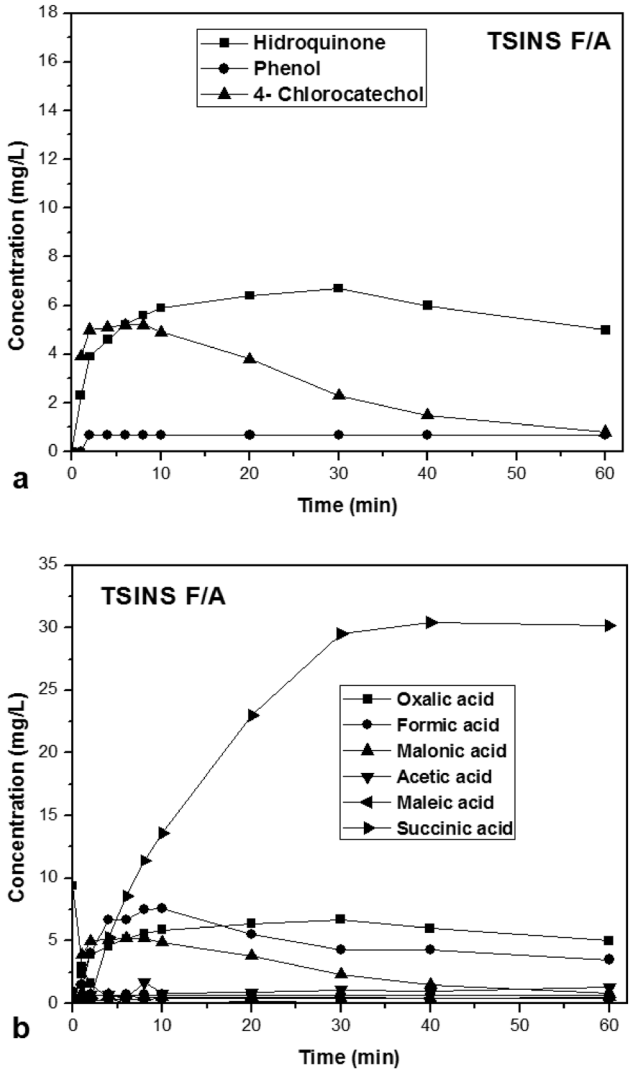

Fig. 16 Effect of air flow during calcination on the 4-Chlorophenol oxidation product distribution obtained when using the TiO_2-SiO_2 monoliths prepared with the addition of the Ti as a sol

Table 2 TOC and mineralization percentages of 4-Chloropenol

Total organic carbon (TOC) Sample	mg/L	4-CP mineralization
Initial solution (4-CP)	121	
TSIN	15.9	86.9
TSIN F/A	16.5	88.2
TSINS	43.4	64.2
TSINS F/A	109.8	9.3

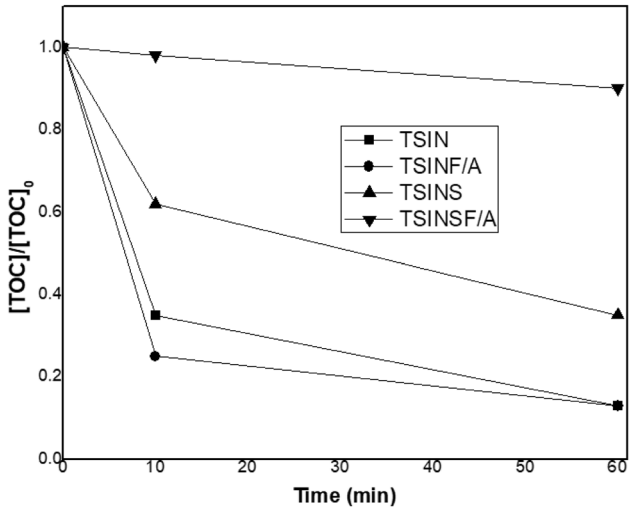

Fig. 17 Initial and final behavior of mineralization of the 4-chlorophenol

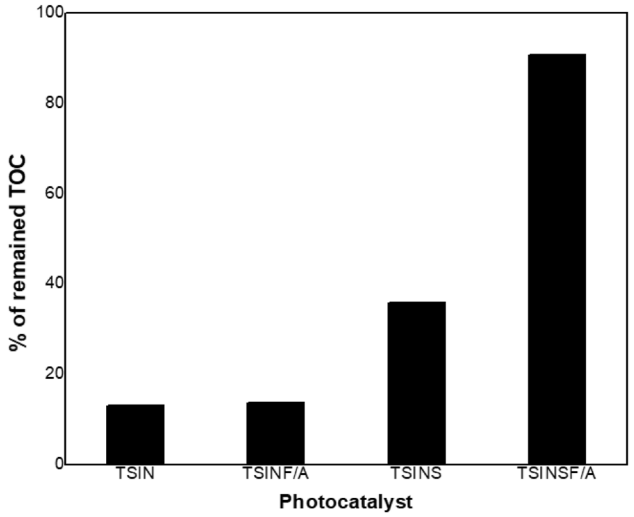

Fig. 18 Remained TOC after 60 min of reaction with the different materials

Table 3 Kinetic data of photocatalytic reactions

Material	K_a (mol/L*s)	K_{ads} (L/mol)
TiO_{2EISA}	1.96×10^{-6}	1.26×10^{2}
Degussa P25	1.72×10^{-7}	4.31×10^{3}
TSIN	1.66×10^{-7}	5.34×10^{3}
TSINS	3.33×10^{-7}	2.92×10^{3}
TSIN F/A	1.00×10^{-6}	1.65×10^{3}
TSINS F/A	2.08×10^{-6}	6.88×10^{2}

Acknowledgements The authors acknowledge for financial support through projects: CIC-UMSNH 4624369, Consejo Nacional de Ciencia y Tecnología (CONACYT-México) 269093. Manuel Robles-Melgarejo thanks CONACYT-México for scholarship 175479 and Facultad de Ingeniería Química of the Universidad Michoacana de San Nicolás de Hidalgo (FIQ-UMSNH). The technical support of Carlos Ornelas, Victoria Lucke and Rosaura Peña Calixto is also acknowledged.

Authors contributions "MR performed the synthesis and test of the materials, wrote the manuscript, analyzed and interpreted the obtained data. JE was the project manager, he proposed the method of synthesis and characterization of the materials, he reviewed the structure of the manuscript and the results obtained, making the pertinent corrections. RN was the co-director of the project, she analyzed the samples resulting from photocatalytic activity by liquid chromatography, reviewed and corrected the manuscript. SJ performed the thermogravimetric analysis of the samples and analyzed the data obtained. JL contributed to the photocatalytic activity tests and in the analysis of the data obtained by X-ray diffraction and scanning electron microscopy. RR contributed to the analysis of reaction kinetics and was a major contributor in writing the manuscript. All authors read and approved the final manuscript." Conceptualization: JEV, MRM; Methodology: JEV, MRM; Formal analysis and investigation: JEV, MRM; Data curates and discussion of results: JEV, MRM, RN, SJGM; Writing—original draft preparation: JEV, MR < , RN; Writing—review and editing: JEV, MRM, RN, JLRC, RR; Resourses: JEV, RN.

Funding Not applicable.

Data availability All data generated or analyzed during this study are included in this published article and its information files are available from the corresponding author on reasonable request.

Declarations

Conflict of interest The authors declare that they don't have competing interests.

References

1. S.S. Prasad, J. Madhavan, Int. J Chemtech. Res. **5**(6), 2970–2974 (2013)
2. H. Wang, Q. Liu, C. You, Appl Catal A. (2019). https://doi.org/10.1016/j.apcata.2018.12.031
3. Y. Ku, R.M. Leu, K.C. Lee, Water Res. **30**(11), 2569–2578 (1996). https://doi.org/10.1016/S0043-1354(96)00147-9
4. A.P. Davis, C.P. Huang, Water Res. **24**(5), 543–550 (1990). https://doi.org/10.1016/0043-1354(90)90185-9
5. R.V. Grieken, J. Maruga, Appl Catal A **312**(1–2), 202–212 (2006). https://doi.org/10.1016/j.apcata.2006.07.003
6. D.S. García-Zaleta, A.M. Torres-Huerta, M.A. Domínguez-Crespo, A. García-Murillo, R.S. Rodrigo, R.L. González, J Nanomater (2016). https://doi.org/10.1155/2016/1805169
7. O. Avilés-garcía, J. Espino-valencia, R. Romero, J.L. Rico-cerda, M. Arroyo-albiter, R. Natividad, Fuel **198**, 31–41 (2017). https://doi.org/10.1016/j.fuel.2016.10.005
8. E. Pabón-Gelves, S. Borja-Ordóñez, J. Ordóñez-Loza, A. Ramírez-Vélez, Revista EIA **19**, 123–132 (2013). https://doi.org/10.24050/reia.v10i19.502
9. K. Ishizaki, S. Komarmeni, M. Nanko, *Porous Materials. Process Technology and Applications* (Kluwer Academic Publishers, Amsterdam, 1998)
10. J. Retuert, R. Quijada, V. Arias, M. Yazdani-Pedram, J. Mater. Res. **18**(2), 487–494 (2003). https://doi.org/10.1557/JMR.2003.0062
11. L. Galeano, J.A. Navío, G.M. Restrepo, J.M. Marín, Informacion Tecnologica **24**(5), 81–92 (2013). https://doi.org/10.4067/S0718-07642013000500010
12. O. Avilés-garcía, J. Espino-valencia, R. Romero, J.L. Rico-cerda, R. Natividad, R. Natividad, Int. J. Photoenergy (2014). https://doi.org/10.1155/2014/210751
13. Z. Li, B. Hou, Y. Xu, D. Wu, Y. Sun, W. Hu, F. Deng, J. Solid State Chem. **178**(5), 1395–1405 (2005). https://doi.org/10.1016/j.jssc.2004.12.034
14. S. Watanabe, X. Ma, C. Song, J. Phys. Chem. C **113**(32), 14249–14257 (2009). https://doi.org/10.1021/jp8110309
15. Y. Castro, J. Mosa, A. Durán, Cerámica y Vidrio. Bol. Soc. Esp. Ceram. Vidrio **53**(2), 171–178 (2014)
16. G. Zu, J. Shen, W. Wang, Y. Lian, L. Zou, Y. Zhang, B. Liu, F. Zhang, J. Supercrit. Fluids **106**, 145–151 (2015). https://doi.org/10.1016/j.supflu.2015.06.001
17. S. Islam, N. Bidin, S. Riaz, R.A. Rahman, S. Naseem, F.M. Marsin, Sensor. Actuat. B Chem. **221**, 993–1002 (2015). https://doi.org/10.1016/j.snb.2015.06.095
18. M.C. Fuertes, G.J. Soler-illia, C. Ato, B. Aires, Chem. Mater. **9**, 2109–2117 (2006). https://doi.org/10.1021/cm0527064
19. N. Nishiyama, K. Kozasa, S. Yamazaki, Appl. Catal. A **527**, 109–115 (2016). https://doi.org/10.1016/j.apcata.2016.09.001
20. E. Pino, M.V. Encinas, J. Photochem. Photobiol., A **242**, 20–27 (2012). https://doi.org/10.1016/j.jphotochem.2012.05.019
21. Y.R. Smith, K.J.A. Raj, V.R. Subramanian, B. Viswanathan, Colloid Surf. A-Physicochem. Eng. Asp **367**(1–3), 140–147 (2010). https://doi.org/10.1016/j.colsurfa.2010.07.001
22. A. Shojaie, M. Fattahi, S. Jorfi, B. Ghasemi, International Journal of Industrial Chemistry (2018). https://doi.org/10.1007/s40090-018-0145-4
23. J. Fern, D. Cazorla, Applied Catalysis A. General **564**(July), 123–132 (2018). https://doi.org/10.1016/j.apcata.2018.07.024
24. H. Joon, S. Kye, H. Ji, H. Jung, J. Bo, Applied Catalysis A. General **558**(March), 9–17 (2018). https://doi.org/10.1016/j.apcata.2018.03.009
25. R. Regalado-raya, R. Romero-romero, O. Avilés-garcía, J. Espino-valencia, Int. J. Photoenergy (2018). https://doi.org/10.1155/2018/8478240
26. L. Mahoney, R.T. Koodali, Materials **2014**(7), 2697–2746 (2014). https://doi.org/10.3390/ma7042697
27. M.A. Carreon, V.V. Guliants, Microreview (2005). https://doi.org/10.1002/ejic.200400675
28. A. Mills, S. Morris, J. Photochem. Photobiol., A **71**(1), 75–83 (1993). https://doi.org/10.1016/1010-6030(93)87012-C
29. U. Stafford, K.A. Gray, P.V. Kamat, J. Phys. Chem. **98**(25), 6343–6351 (2002). https://doi.org/10.1021/j100076a019
30. L. Rideh, A. Wehrer, D. Ronze, A. Zoulalian, Industrial & amp. Engineering Chemistry Research **36**(11), 4712–4718 (1997). https://doi.org/10.1021/ie970100m
31. S.L. Orozco-Cerros, J.M. Barrera, Redalyc. Tecnol. Ciencia Ed. (IMIQ) **25**(2), 113–121 (2010)
32. Z. Sun, C. Bai, S. Zheng, X. Yang, R.L. Frost, Appl. Catal. A **458**, 103–110 (2013). https://doi.org/10.1016/j.apcata.2013.03.035
33. X. Ding, Y. Guo, Y. Deng, C. Wang, M. Li, Z. Wang, Mater Lett **60**(12), 1515–1518 (2006). https://doi.org/10.1016/j.matlet.2005.11.062
34. F. Leonardo-Alféreza, J. Jairo-Olayaay, J. Hernando-Bautista, Bol Soc Esp Ceram V **57**(2018), 195–206 (2018). https://doi.org/10.1016/j.bsecv.2018.02.001
35. A. Amlouk, L. El Mir, S. Kraiem, S. Alaya, J. Phys. Chem. Solids **67**(7), 1464–1468 (2006). https://doi.org/10.1016/j.jpcs.2006.01.116

36. E. Pabón, J. Retuert, R. Quijada, A. Zárate, Micropor. Mesopor. Mater. **67**(2–3), 195–203 (2004). https://doi.org/10.1016/j.micromeso.2003.10.017
37. T. Ohno, K. Sarukawa, K. Tokieda, M. Matsumura, Morpho. J. Catal. **203**(1), 82–86 (2001). https://doi.org/10.1006/jcat.2001.3316
38. Z. Liu, F. Chen, P. Fang, S. Wang, Y. Gao, F. Zheng, Y. Liu, Y. Dai, Appl. Catal. A **451**, 120–126 (2013). https://doi.org/10.1016/j.apcata.2012.11.020
39. E. Martín Del Campo, J.S. Valente, T. Pavón, R. Romero, A. Mantilla, R. Natividad, Ind. Eng. Chem. Res. **50**(20), 11544–11552 (2011). https://doi.org/10.1021/ie200412p
40. J.S. Valente, F. Tzompantzi, J. Prince, Appl. Catal. B **102**(1–2), 276–285 (2011). https://doi.org/10.1016/j.apcatb.2010.12.009
41. G. Sivalingam, M.H. Priya, G. Madras, Appl. Catal. B **51**(1), 67–76 (2004)
42. Y. Arai, K. Tanaka, A.L. Khlaifat, J Mol Catal A Chem **243**(1), 85–88 (2006). https://doi.org/10.1016/j.molcata.2005.08.016
43. A. Payan, M. Fattahi, B. Roozbehani, Appl. Surf. Sci. (2018). https://doi.org/10.1016/j.apsusc.2017.10.149
44. R. Alimoradzadeh, A. Assadi, S. Nasseri, M.R. Mehrasbi, Iran. J. Environ. Health Sci. Eng. **9**(12), 1–8 (2012). https://doi.org/10.1186/1735-2746-9-12
45. J. Theurich, M. Lindner, D.W. Bahnemann, Langmuir **12**(26), 6368–6376 (1996). https://doi.org/10.1021/la960228